

Comparative study of the mechanism
underlying orientation selectivity in mammals

Yamni Mohan

Contents

1 Acknowledgements	5
2 Abstract	6
3 Introduction	7
4 Methods	9
4.1 Experimental Animals	9
4.2 Surgery and Anaesthesia	9
4.3 Optics	11
4.4 Monitoring Protocol	11
4.5 Electrophysiological Recordings	11
4.5.1 Single Electrode Recordings- Primary Visual Cortex .	11
4.5.2 Single Electrode Recordings- Superior Colliculus . .	12
4.5.3 Multielectrode Electrode Recordings- Primary Visual Cortex	12
4.6 Stimulus Presentation	12

4.6.1	Stimulus used for experiment one	12
4.6.2	Bar stimuli	13
4.6.3	Grating stimuli	13
4.6.4	Stimuli for multielectrode recording	14
4.7	Histology	14
4.7.1	Cresyl Violet Staining	14
4.7.2	Track Reconstruction	14
4.8	Data Analysis	15
4.8.1	Post- stimulus time histograms	15
4.8.2	Defining response	15
4.8.3	Measures of orientation tuning	16
4.8.4	Spatial Frequency Tuning	17
4.9	Optical Imaging of Intrinsic Signals	17
4.9.1	The apparatus	17
4.9.2	Stimulus generation and presentation	18
4.9.3	Analysis of Intrinsic Signals	18
I	Subcortical orientation biases	19
5	Orientation anisotropies in the inputs to the primary visual cortex of macaques	20
5.1	Abstract	21
5.2	Introduction	22

5.3	Methods	26
5.3.1	Data Collection	26
5.3.2	Data Analysis	28
5.4	Results	34
5.5	Discussion	45
5.6	Conclusions	50
6	Orientation tuning in the Tree Shrew superior colliculus	51
6.1	Abstract	52
6.2	Introduction	53
6.3	Methods	55
6.3.1	Electrophysiology	55
6.3.2	Stimuli	56
6.3.3	Data Analysis	58
6.4	Results	59
6.5	Discussion	64
6.5.1	Anatomical Relevance	66
6.5.2	Comparison with previous tree shrew studies	68
6.5.3	Comparison with previous superior colliculus studies .	70
6.5.4	Comparison with the geniculostriate system of cats and macaques	71
6.5.5	Conclusion	72

**II Insights from the Tree Shrew Primary Visual Cor-
tex** **73**

References **74**

Chapter 1

Acknowledgements

Chapter 2

Abstract

Chapter 3

Introduction

Over the years, sub-cortical orientation biases have been shown to play a significant role in two key areas of study in the primary visual cortex. The first is its role in generating sharp orientation selectivity in the cortex and second is its role in generating the cortical architecture. In my thesis, I aim to further characterise the sub-cortical orientation biases and examine their role in visual processing. In the first part of my thesis, I would like to characterise the origin of the biased sub-cortical input to the cortex. There is debate as to exactly when in visual processing the orientation bias observed in the cortical input is generated. Some studies claim that this orientation bias is generated early on in the visual processing: namely the retina. Some others claim that these biases are generated through a mechanism such as excitatory convergence in the cortex. This part probes this question in two ways.

Chapter 6

This chapter examines if there is a preponderance of a particular orientation in the cortical inputs. If the orientation bias in the cortical input is generated by Hubel and Wiesel type excitatory convergence — where circular LGN receptive fields converge on to a V1 neuron — we would expect that inputs to the cortex don't show any preferences (i.e. the orientations of the inputs will be randomly distributed.). Many studies however, have shown that RGCs and LGN neurons are preferentially tuned to the radial orientation (the orientation of the line joining the center of the receptive field to the centre of visual field). If the orientation bias in the inputs is derived from the retina instead, then this

Chapter 4

Methods

4.1 Experimental Animals

4.2 Surgery and Anaesthesia

All experiments have ethics approval. This study looked at cortical responses to visual stimuli in three different species, cats, macaques and tree shrews. This chapter outlines the methodology that was common in all three animals. Experiment specific methodology is incorporated in the individual chapters.

In all animals, initial anaesthesia was induced using a mixture of ketamine and xylazine (Varied dosage). Once the animals were anaesthetised, tracheostomy and venous cannulation (cephalic in cats and macaques; femoral in tree shrews) was completed. During the experiment, anaesthesia was maintained using a gaseous mixture containing nitrogen, oxygen and carbon-di-

oxide (See table for dosage). Paralysis was established using an intravenous bolus of norcuron and was maintained using vecuronium administered intravenously. The animal's body temperature was maintained between 36-37 degrees using a servo controlled heating blanket. ECG and EEG were monitored throughout the experiment and the level of anaesthesia was adjusted accordingly. Following initial surgery, a craniotomy and durotomy were conducted over the location of the primary visual cortex (V1, see table for horsley-clarke co-ordinates.). Once recordings were completed, the experiment was terminated by administering the animal an overdose of pentobarbitone (dosage) intravenously. The animal was then perfused intracardially using phosphate buffer, a paraformaldehyde solution; the brain was removed and stored in a solution of 25 percent sucrose for cryoprotection. The brain was later processed for histology.

4.3 Optics

4.4 Monitoring Protocol

4.5 Electrophysiological Recordings

4.5.1 Single Electrode Recordings- Primary Visual Cor-tex

Electrophysiological measurements were done using high impedance tungsten micro-electrodes (betn 4 and 18 megaohms.). The electrodes were inserted into the cortex and were plugged into a pre-amp. The signal from the pre-amp was passed through a antialiasing filter (high cut-off= 5000 Hz), a humbug was used to reduce 50 Hz line noise, and the resulting signal was passed through a band-pass filter (between 300 and 3000 kHz). The signal was digitised at 22.5 kHz using a analog to digital converter. The data was recorded using the spike 2 software. In order to ensure that our recordings were actually spiking outputs of neurons, we also made sure that we had a reasonable signal to noise ratio. A template of the spikes was built using spike 2 software and used for online analysis. The original signal was stored for later analysis.

4.5.2 Single Electrode Recordings- Superior Colliculus

4.5.3 Multielectrode Electrode Recordings- Primary Visual Cortex

4.6 Stimulus Presentation

Stimulus was presented on a barco monitor (Frame rate= 80 Hz). All stimulus was generated in SDL and presented using ViSaGe stimulus generator. For the first experimental chapter, we used full field square wave gratings. For the rest of the experimental chapters, we used bars and smaller, sinusoidal gratings.

4.6.1 Stimulus used for experiment one

For the first experimental chapter, 'Radial bias in the inputs to the cortex', the anaesthetised animal was presented full-field, square wave gratings with SF= between 1 and 4 cpd. The temporal frequency was 2.2 Hz and contrast was set at 100 percent. The stimulus was presented for 7.3s followed by an interstimulus interval of 10s. The gratings that were presented were of different orientations between 0 and 157.5 degrees in 22.5 degree steps.

4.6.2 Bar stimuli

For all other experimental chapters, initially, a bar was presented to determine the orientation of a unit. As layer 2/3 neurons (in shrews; layer 4 in cats) were sharply tuned to orientation, they only responded to bars of certain orientations. For layer 4 neurons in shrews, thinner bars were used to determine orientation preference. The bars were also varied in length to account for length response functions, contrast and speed in order to optimise the stimuli and only study the effect of the dimension that was changed. During the experiment, optimum orientation was determined by looking at the peak responses of the orientation response obtained using a PSTHs.

4.6.3 Grating stimuli

Once the orientation of the stimulus was gauged, the animal was presented with grating stimuli to determine spatial frequency tuning of the neuron. To get spatial frequency tuning of the neurons, orientation, contrast, size of the grating were optimised and the spatial frequency was varied in 0.1 cpd steps (for tree shrews). This was repeated at four different orientations 45 degrees apart. The differences in the spatial frequency tuning between different orientations was examined.

4.6.4 Stimuli for multielectrode recording

4.7 Histology

After the experiment, the tissue was processed for histology as follows. The brain was stored in a 25 percent sucrose solution until it sank. This was to ensure that the tissue was cryoprotected. After this, the brain was blocked so that only the areas of interest was processed. The brain was frozen in a cryostat and 50 micron sections were made. The sections were mounted on gelatinised slides. Once the sections were dry, they stained.

4.7.1 Cresyl Violet Staining

First the sections were dehydrated using increasing concentrations of ethanol. Then, chloroform was used to defatten the sections. This was followed by rehydrating sections in decreasing concentrations of ethanol. THe sections were then stained using Cresyl Violet Acetate solution (0.1 perc, Sigma) and differentiated using a solution of 5 percent acetic acid in 95 percent ethanol. It was then dehydrated using increasing concentrations of ethanol and fixed in histolene. The slides were then coverslipped.

4.7.2 Track Reconstruction

In order to reconstruct electrode tracks, we located the electrolytic lesions/ pontamine lesions that we made under the microscope and digitised those

sections. The shrinkage was calculated by comparing the recorded and observed distances between lesions. This shrinkage calculation was used to calculate the actual depth of the units recorded. Based on the location of the unit, it was classified as layer 4 or layer 2/3 unit and this classification was used for further analysis.

4.8 Data Analysis

4.8.1 Post- stimulus time histograms

We have spikes based on a template. The response to a particular stimulus is arranged in a PSTH. The X-axis of a PSTH is time after stimulus has been presented and the Y-axis is the response (usually measured as spike counts or spike rates). The spikes that occur during stimulus presentation are binned in 20 ms bins and presented as a histogram and this is used for further analysis.

4.8.2 Defining response

When presented with a bar, response is the spike rate. Getting a maximum response just means getting maximum spike rate while a given stimulus crosses the receptive field. Whereas, this is not the same for gratings. A unit based on whether it demonstrates linear summation over its receptive field or not responds differently to a grating. For example, a simple cell gives a

modulated response to a grating whereas a complex gives an unmodulated response. These response properties are so distinct that this is one of the key criterias used to distinguish between the two types of neurons (see Skottun et al., 1991).

Therefore, the response of units to gratings are plotted in a PSTH and a discrete fourier transform using a fast fourier transform is run on the resulting trace (using custom code in MATLAB; see appendix). The F0 component thus obtained will equal the mathematical mean of the trace. The F1 component would be related to the temporal frequency of the stimulus. Since simple cells show half-wave rectification, the F1 component of the FFT is doubled and this is taken as the F1 component of the response. The modulation ratio will be calculated as calculated by Van Hooser et al., 2013 (for better comparability) and if it is greater than 1, then the unit is considered complex. If it is less than 1, then it is considered simple. The response magnitude will be used accordingly.

4.8.3 Measures of orientation tuning

Two separate measures of orientation tuning will be calculated; the orientation selectivity ratio, which gives information on the optimum and orthogonal orientations and the circular variance which gives an indication of the circularity of the responses of the neuron. The formulas for these are as shown below.

4.8.4 Spatial Frequency Tuning

Spatial frequency tuning curves were fit to the spatial frequency responses of a neuron. The SF tuning curve is ideally defined by a difference of Gaussian curve as specified in REFERENCE.

4.9 Optical Imaging of Intrinsic Signals

4.9.1 The apparatus

Macroscope and camera

The chamber

The Illumination system

Optical imaging of intrinsic signals was a technique established in the 1990s to look at the organisation of the cortex on a scale greater than the individual neuron level. It consists of fast-scanning ccd camera which has two lenses attached face to face to it. This setup allows the user to specify a narrow depth of focus. The camera essentially looks at the changes in reflectance of the blood signal in response to a visual stimulus. It is based on the principle that the amount of oxygen present in the blood affects its reflectance. In response to neuronal activity, the amount of oxygenated haemoglobin in the blood decreases and the amount of deoxygenated haemoglobin in the blood increases. At certain wavelengths of light, this difference can be dis-

tinguished. At the isosbestic wavelength (570 microns), the reflectance of oxy and deoxy haemoglobin remains the same. At higher wavelengths, however, the difference in reflectance varies causing there to be change in signal. The reflectance of a region of cortex decreases in response to neural activity and this signal is captured in optical imaging. Accordingly, in response maps, activity is represented by dark patches.

4.9.2 Stimulus generation and presentation

4.9.3 Analysis of Intrinsic Signals

Obtaining single condition maps

Obtaining orientation maps

Part I

Subcortical orientation biases

Chapter 5

**Orientation anisotropies in the
inputs to the primary visual
cortex of macaques**

5.1 Abstract

The neurons of the primary visual cortex are arranged in columns based on their orientation preference. The columnar architecture has orientation columns that cycles through all the orientations and converge at a pinwheel centre. It has recently been proposed that both this columnar organisation and the orientation selectivity of individual neurons can be established from broadly tuned subcortical inputs. While this has to some extent been demonstrated in intracellular recordings, the overall nature of these inputs is yet to be studied. In this study, I will be using optical imaging of intrinsic signals to characterise these inputs. The columnar architecture first revealed using extracellular recordings but was further confirmed using optical imaging of intrinsic signals (OI). OI detects the haemodynamic change that accompanies neural activity. A lower level of oxygenated blood would indicate higher activity. Traditionally the signal from the OI is spatially filtered in order to isolate activity in the relevant spatial scale; activity that corresponds to the output of the neurons. Here I use the unfiltered signal to reveal activity that is more congruent with the pre-synaptic and synaptic activity. When examined this way in the anaesthetised macaque primary visual cortex, the unfiltered signal is tuned to the radial orientation (the orientation the receptive field makes with the visual field). These results show that inputs to the cortex are biased toward the radial orientation, a bias that has been observed in both the retina and LGN of the macaque.

5.2 Introduction

Neurons in the primary visual cortex are tuned to orientation and these orientation tuned neurons are organised in columns. Hubel and Wiesel (1962) showed that neurons in Area 17 of cats were sharply tuned to orientation. These neurons were also grouped into neurons of similar orientation. This was then repeated in macaques. Hubel and Wiesel suggested their excitatory convergence model for orientation tuning. This model suggests that orientation tuning in the primary visual cortex is established by the feedforward convergence of inputs from neurons arranged in a row in the lateral geniculate nucleus (LGN). Now, the orientation selectivity and the columnar architecture is a widely accepted characteristic of the primary visual cortex of most species (see mouse work for an alternative scheme, (Reference)). However, the question remains as to whether both these properties arise from the same mechanism.

A study by Sur et al. (2001) showed that simple feedforward mechanisms were not effective in establishing the columnar architecture observed in the primary visual cortex. Where they routed signals from the V1 to the auditory cortex, they found that orientation tuning was sharpened (although not enough) by the feedforward mechanism but the cortical architecture of V1 was not reflected in the auditory cortex, implying that intracortical intervention was necessary for establishing cortical architecture as we know it. A new theory (Vidyasagar and Eysel, 2015) suggested that both the ori-

tation tuning of cortical neurons and cortical architecture can be established by sharpening biases that originate earlier on in the visual system.

Let us examine the way the visual system processes colour data. Colour is encoded in the retina by cones with broad sensitivities that act in an opponent manner to each other. So, there is the red/ green opponent system and blue/ yellow opponent system encoded by the L, M and S cones. These cones are activated by a light of a large range of wavelengths. Neurons in the primary visual cortex (V1) that are tuned to colour however, only respond to particular wavelengths of light. This tuning in the primary visual cortex arises from a sharpening of the broader bias established in the retina. A similar mechanism has been reported for other features that have been observed in the V1. Neuronal properties such as ocular dominance and phase selectivity (on/off) can all be explained by biases established by biases observed in the retina. A similar mechanism may be proposed for orientation selectivity.

The case of orientation selectivity is more complex than ocular dominance or phase selectivity. The nature of ocular dominance and phase selectivity is such that the seed for their tuning in the retina is quite intuitive and commonly accepted. Inputs may either be from the right eye or the left eye. They may arise from a ganglion cell that receives inputs from an on or off bipolar cells. These biases are well characterised in the literature. In the case of orientation selectivity however, the sub-cortical biases are not so obvious. While many studies have shown that sub-cortical neurons are indeed biased for orientation (eg: see Levick and Thibos, 1980; Vidyasagar and Urbas,

1982) it is still not widely accepted. Several studies continue to argue that orientation selectivity is first generated in the primary visual cortex through some variant of the excitatory convergence model. Further, the exact nature of the bias is still questioned. Some studies suggest that there is radial orientation bias in the retina. Some others suggest that there is a preponderance of the horizontal and vertical orientation biases (the oblique effect). Rovamo et al (1978) showed an eccentricity dependence of perceptual bias with the central vision showing oblique effect and peripheral vision showing the radial bias. One study in the cat area 17 showed that first order neurons in layer 4 of the cortex were tuned to cardinal orientations. Cardinal orientations were defined as vertical, horizontal or radial. It could be that the retinal neurons are tuned for one of these cardinal orientations which are reflected in the first order neurons in the cat visual cortex.

One of the key tools that have been instrumental in revealing cortical architecture is optical imaging of intrinsic signals (OI). Introduced in the 90s, OI helped visualise the cortical orientation columns converging at a pinwheel centre. OI images the haemodynamic change that accompanies neural activity and is based on the principle that deoxygenated blood reflects less light than oxygenated blood. This means that activity is observed as dark areas in the response maps. The haemodynamic change that is recorded using OI is akin to the BOLD (Blood Oxygen Level Dependent) response observed in fMRI. Studies have suggested that the BOLD response is predominantly a reflection of the pre-synaptic and synaptic activity with the extracellular,

spiking activity forming a very small part of the response. The OI images that we observe are reflections of the spiking activity. This is because, traditionally OI signal is spatially filtered to only display the spiking activity. Here, I aim to use the non-filtered signal to study the pre-synaptic and synaptic activity in the macaque V1. Using optical imaging helps reveal any larger scale organisation that cannot be otherwise observed.

Hypothesis:

- If cortical orientation tuning and architecture were derived from broadly orientation inputs, then the unfiltered OI response will be tuned to one of the cardinal orientations.
- If however, the orientation biases in the inputs were derived from a mechanism such as excitatory convergence, the unfiltered OI response will show no such preponderance.

5.3 Methods

5.3.1 Data Collection

Stimulus

During the experiment OI maps were calculated in response to visual stimulation. Visual stimulus was generated using the Visual stimulus generator (SDL, Cambridge Research Systems, UK) and presented on a Barco monitor (Reference Calibrator plus; Barco Video and Communications, Belgium). The monitor was positioned at 57 cm from the animal. The stimulus presented was a full field, square-wave, bidirectional, drifting grating ($SF = 1\text{-}4$ cpd, $TF = 1.5$ Hz, Michelson contrast = 100%). The orientation of the grating changed sequentially in 22.5 degree steps from 0 degrees to 157.5 degrees. A 0 degree grating was a horizontal grating moving bidirectionally. The stimulus was presented for 7.3 seconds followed by an interstimulus interval of 10 seconds where the animal viewed a blank screen.

Optical Imaging of intrinsic signals

Optical imaging of intrinsic signals was used to obtain the haemodynamic change related to the neural response to orientation stimuli. The OI setup involved two camera lenses (Canon) arranged in a tandem fashion (Reference) connected to a CCD camera. The tandem lens arrangement allowed for a narrow plane of focus. An LED light source was used to illuminate the

cortical surface. Before stimulus presentation, a high contrast, green image of the surface of the imaged cortex was obtained by illuminating the cortical surface with green light (filter wavelength=545 nm). This provided us with cortical landmarks which were later used in determining the locations for electrode tracks for topographical recordings. Following this, the plane of focus of the camera setup was changed to between 550-700 microns beneath the surface of the cortex and the wavelength of the illuminating light was changed to 630 nm. 18 frames, each 400 ms long were collected for each stimulus presentation. The signal to noise ratio was enhanced by acquiring data over 50 trials collected in 10 blocks of 5 trials each. Where possible, given the condition of the imaged area and the animal, the experiment was repeated a second time. Using the OI data acquisition system, each block was exported as a MATLAB file. Each individual frame in a block was the average of that frame for 5 trials. Analysis was conducted on the exported MATLAB files.

Topographical recordings

The study of radial bias requires the careful plotting of receptive field locations in relation to their cortical location. High impedance tungsten microelectrodes (12 MOhm, FHC Inc) were used to record from predetermined locations on the imaged cortical surface). The analog signal was amplified and filtered (Amplifier specs; Gain = x10,000; Band pass between 300 and 3000 Hz). The filtered signal was then visualised using an oscilloscope (Os-

cilloscope specs) and fed through an audio speaker to aid in plotting the receptive fields. First the foveal location (if visible) and the optic nerve with blood vessel markers were plotted using a fundus camera (Fundus Camera specs). Then the location of the receptive fields were carefully hand plotted using handheld stimuli from the corners of the imaged area (See figure 3). In between each electrode penetration, where possible, the location of the fovea and optic nerve head were replotted in order to account for eye movement.

5.3.2 Data Analysis

Image Analysis

Of the 18 frames collected, the mean of 14 frames (frames 3-16) was calculated for individual blocks in each stimulus condition. The first frame was then subtracted from the averaged frames for each stimulus condition. The mean of 10 blocks was then calculated. This gave us the unfiltered single condition maps (referred to as veridical SCMs). Traditionally, when analysing the images obtained using optical imaging of intrinsic signals, the following method is used. The veridical SCMs are band pass filtered using the method described in figure 6.1. The unfiltered map is first low pass filtered using a large spatial filter (Gaussian filter, sigma= 312.5 microns). This removes the low frequency information. By subtracting the low pass image calculated above from the original image, we preserve only the high spatial frequency information. This will be called the high-pass single condition map. The

high pass single condition map is then smoothed with a gaussian filter with a smaller sigma value (100 microns). This is the band pass filtered single condition map or more commonly just referred to as the single condition map (these will be referred to as filtered SCMs throughout this thesis). The filtered SCMs are then vector averaged to look at the angular mean of individual pixels (Swindale). This will produce the traditional filtered orientation tuning maps. In our study, we also vector averaged the veridical SCMs. We called the maps derived this way the veridical orientation maps (see appendix for code).

Analysis of electrophysiological recordings

In order to determine the azimuth and elevation of receptive fields obtained during the experiment, we set the co-ordinates of the fovea at (0,0). We obtained the azimuth and elevation of receptive fields in relation to the centre. If there were eye movements during the experiment, the Cartesian co-ordinates of the foveal location was set as (0,0). The horizontal and vertical distances of the receptive field centre from the foveal location were calculated. The azimuth and elevation of receptive fields were then calculated as the horizontal and vertical angles subtended by the animals eyes to the receptive field centre. If there were eye movements during the experiment, (0,0) was assigned to the new foveal location. Receptive field locations were replotted in relation to foveal locations plotted closest to the recording in order to get as accu-

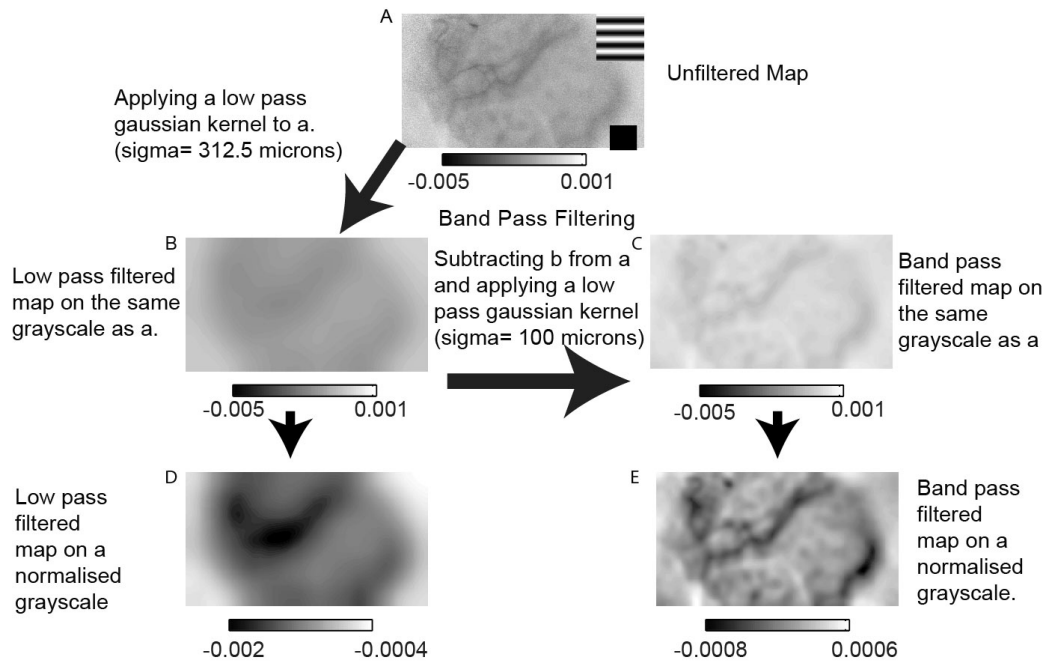


Figure 5.1: Figure 1: Description of the filtering process. A low pass Gaussian filter ($\sigma=312.5 \mu\text{m}$) is applied to the unfiltered single condition map (SCM; (a)) to obtain the low pass filtered map (b). The map in (b) is subtracted from the map in (a) and then another low pass Gaussian filter ($\sigma=100 \mu\text{m}$) is applied to the subtracted image to get the filtered SCM (c). The images in b and c are displayed on the same gray scale (displayed just below the maps). In parts (d) and (e), the same maps are normalised to their respective maximum and minimum values (displayed along with the grayscale below the maps). (e) is the classical filtered SCM. The scale bar is 1mm.

rate a receptive field location as possible. This then allowed us to accurately determine the azimuth and elevation of the receptive fields.

Using the receptive field locations thus calculated, we used the eccentricity, azimuth and elevation values to calculate iso azimuthal and iso elevation lines on the cortex (see appendix 6.2). We used the magnification factor calculations in the macaque cortex published by Dow et al (1960) to calculate the magnification factor – how many degrees in visual space one would traverse if we moved 1 mm in cortical space and the inverse magnification factor; how far one needs to move on the cortex to traverse 1 degree in visual space, given the eccentricity of the receptive fields. These values were used to calculate the azimuth and elevation of points on the cortex that were spaced 375 microns apart. The radial angle of each of the points was calculated given the azimuth and elevation of their RF locations and averaged to calculate the average radial angle of the imaged area.

Defining Region of Interest

As described above, the azimuth and elevation of points on the cortex that were 375 microns were calculated. These points were defined as Region of interest (ROI) centres. The ROIs were then defined as a 750 micron square around the ROI centre. The radial angle of the centre was taken to be the radial angle for each pixel in the ROI. The average optimum orientation of the individual pixels in the ROI was calculated and then compared to the radial angle of the ROI from both the veridical and filtered orientation maps.

The difference of the radial angle and optimum orientation of the ROI was calculated.

Single pixel analysis

The ROI analysis was used to determine if any of the cortical inputs were dominant in the larger spatial scale. This analysis, by definition is not sensitive enough to pick up any of the inputs that may be present on a smaller spatial scale. Therefore, we also compared the orientation tuning of single pixels to the radial bias of the imaged area. Accordingly, the optimum orientation of the individual pixels was subtracted from the mean radial orientation of the imaged area for the veridical and filtered maps. Further, each pixel was grouped by the SCM for which it gave the maximum response. The pixels were then centred on the radial orientation. This second method of analysis would also allow us to see if individual pixel responses that may be smoothed over the vector averaging process. In both the conditions, the pixels were also grouped according to stimulus condition to see if there was a bias for the horizontal and vertical orientations.

Adjusting for sample size in single pixel analysis

As we were examining the single pixels in multiple orientation maps, there were a large number of pixels. In order to make sure we were not detecting an insignificant effect made significant by sample size, we randomly resampled with replacement from the distribution of pixels in both conditions to see if

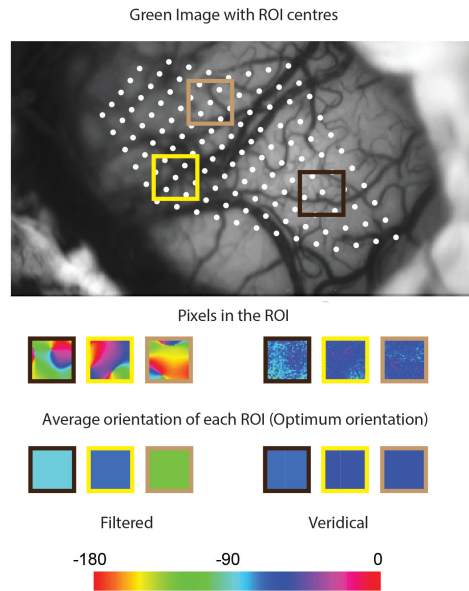


Figure 5.2: Method Figure for ROI

there was an effect at smaller sample sizes. We used two sample sizes (40 and 1000) sampled 1000 times and calculated the chi-square of the 1000 trials.

5.4 Results

We recorded OI and topographical recordings from 5 monkeys (*Macaca fascicularis*, all male, aged between 2 and 5 years). The results are presented below. All representative data is from one of our animals (MBM5).

Examining Single Condition Maps

Single condition maps show that there is more activity overall in orientations closer to the radial orientations in the veridical maps. Figure 6.3 shows the veridical (a) and the filtered (b) SCMs generated in response to grating orientation (top row) for one animal (MBM5). The star in the veridical SCM indicates the response condition closest to mean radial orientation for this imaged area. In these maps, darker areas indicate activation. Observing the intensities of the response, one can determine that the responses to orientations closer to the radial orientations are higher than the responses to non radial orientations. This is shown quantitatively in the box plots in part c. The intensity values (higher values mean darker) are higher near the radial orientations. A similar trend was observed when the study was repeated again (see parts d,e and f) suggesting that at the radial orientation there is generally more activity. This activity is also broadly tuned as it is observed in a few orientations surrounding the radial orientation.

The filtered single condition maps show little change compared to the veridical SCMs. Observing the filtered SCMs in part Fig 6.3b, one can con-

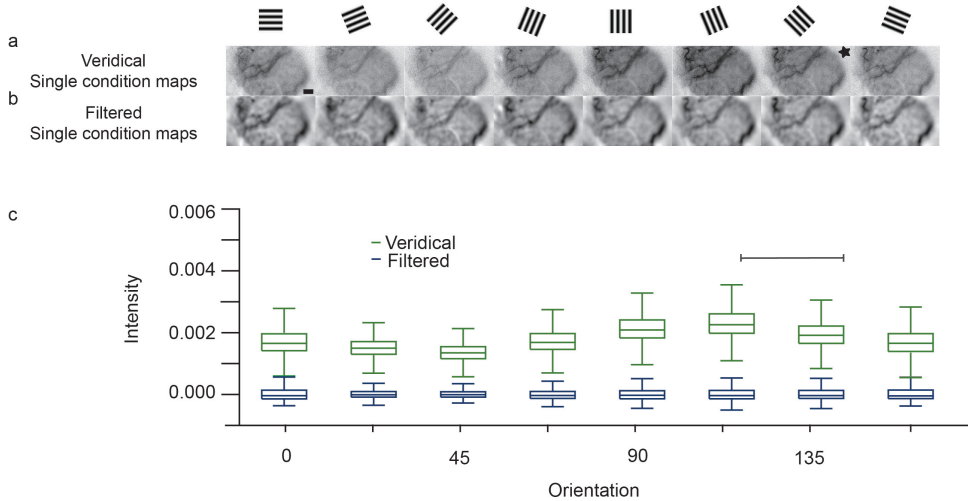


Figure 5.3: Example of filtered and veridical single condition maps.

clude that compared to the veridical maps, the size of the effect seen in filtered SCMs is relatively small. Examining the box plots, the relatively flat distribution of pixels in the box plots when plotted on the same scale as the activity in the veridical maps suggests that there is also no preferred bias in the data. The smaller magnitude of the values is also shown in the displacement of the filtered boxplot series below the veridical series further indicating that not only is there an obvious bias in the responses of the filtered maps, the response that is presented in these SCMs are also smaller in magnitude compared to the unfiltered maps.

Orientation Tuning Maps

The filtered orientation tuning maps resemble the traditional orientation tuning maps whereas the veridical orientation maps are predominantly tuned to

one orientation. Figure 6.4 shows the filtered and veridical orientation tuning maps for the same animal showed in figure 6.3. The filtered orientation map shows orientation columns that converge at a pinwheel centre. The response of the neuron indicated by recordings made at the location indicated by the diamond is shown in panel e. The orientation of this neuron corresponds to the orientation of the column from which it was recorded from. The receptive field locations of the recordings are shown in 6.4b. The pseudo colour scale on the outside of the Cartesian scale is the same scale used in parts c and d. We can see that if we draw a line starting from the centre of gaze, passing through the centre of the receptive field to the colour scale, the colours will correspond to the same colours seen in the veridical map indicating that large areas of the cortex in the veridical maps are tuned to the radial orientation. Results are presented in a similar fashion for all the animals in our study in figure 6.5.

Comparing the radial orientation and optimum orientation of ROIs

When the optimum orientation and the radial orientation were compared, most ROIs were tuned to the radial orientation in the veridical condition. This was not the case in the filtered condition. Figure 6 shows the distribution of the absolute differences between the optimum and radial orientations of the ROIs for the veridical and filtered orientation maps. We find that in the veridical condition, most differences were between 0 and 22.5 degrees (mean=; SE=) suggesting that most of the ROIs were tuned to the radial

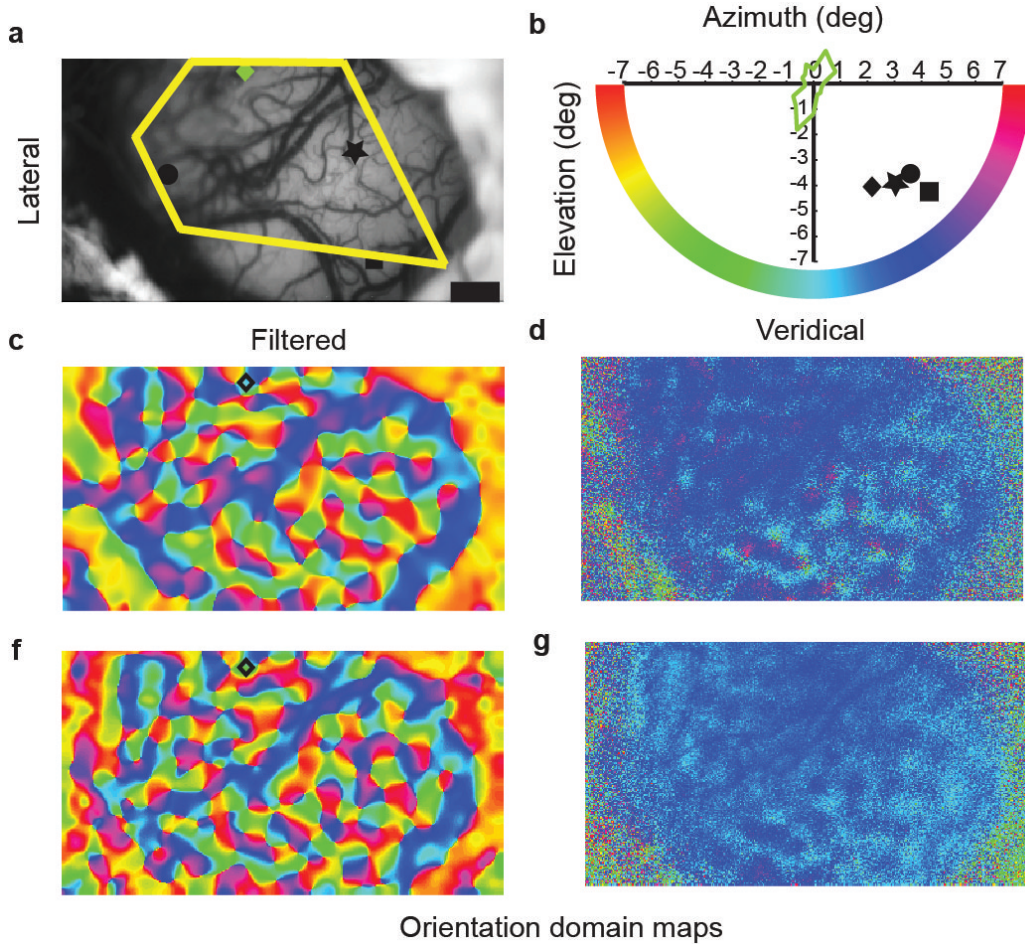


Figure 5.4: Orientation maps from a representative animal. (a) is the green image obtained using the 545 nm green filter to show surface landmarks. The yellow polygon is the area used for ROI and single pixel analysis. The various symbols represent the locations of electrode penetrations. The receptive field locations of the electrode penetrations are represented by their corresponding symbol in (b). The orientation tuning curve overlaid on the axis corresponds to the orientation tuning recorded using a tungsten microelectrode from the location denoted by the diamond (coloured green; maximum response= 40 spks/s). The colour of the orientation tuning curve corresponds to the colour of the optimum orientation of the neuron (circular mean= 257 deg) according to the pseudocolor scale. (c) and (d) are the filtered and veridical orientation tuning maps. (e) and (f) are the same maps obtained when the entire experimental protocol is repeated. The diamonds location is transposed on to the two filtered maps. The optimum orientation obtained from the OI maps was similar to that obtained using electrophysiology (circular mean for OI= 263 deg, average from the two repeats). The optimum orientations of the filtered conditions on the other hand closely correspond to the radial angle of their receptive fields. Scale bar is 1mm.

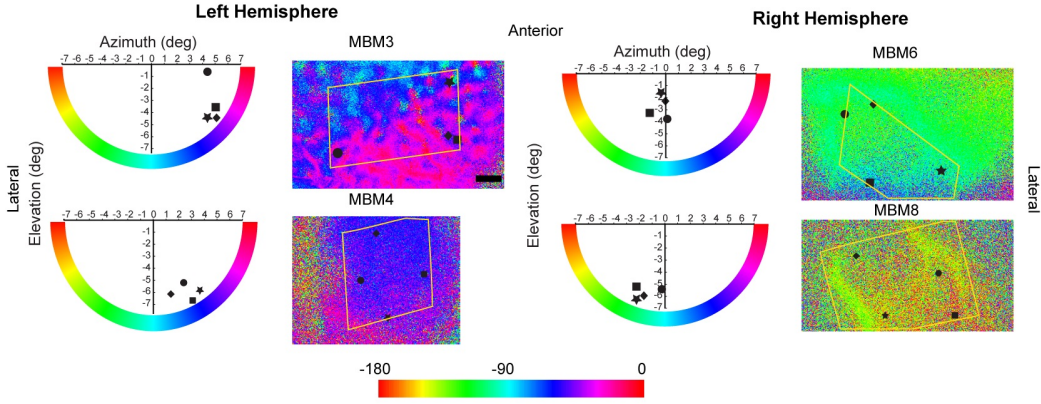


Figure 5.5: The receptive field location, veridical and filtered orientation tuning maps of all the animals (except that showed in figure 6.3) used in our studies. The conventions are as explained figure 6.3.

orientation. In the filtered condition, the mean of the ROIs were further away from zero (mean=; SE=). When a chi-square test was performed, we found that the distribution of absolute differences for the veridical condition was significantly different from a uniform distribution (chi-square=; df=; p). Surprisingly, the absolute differences for the filtered condition were also significantly different from the uniform distribution but to a lesser extent than the veridical condition (chi-square=; df=; p=). The absolute differences for the veridical and the filtered conditions were also significantly different from each other.

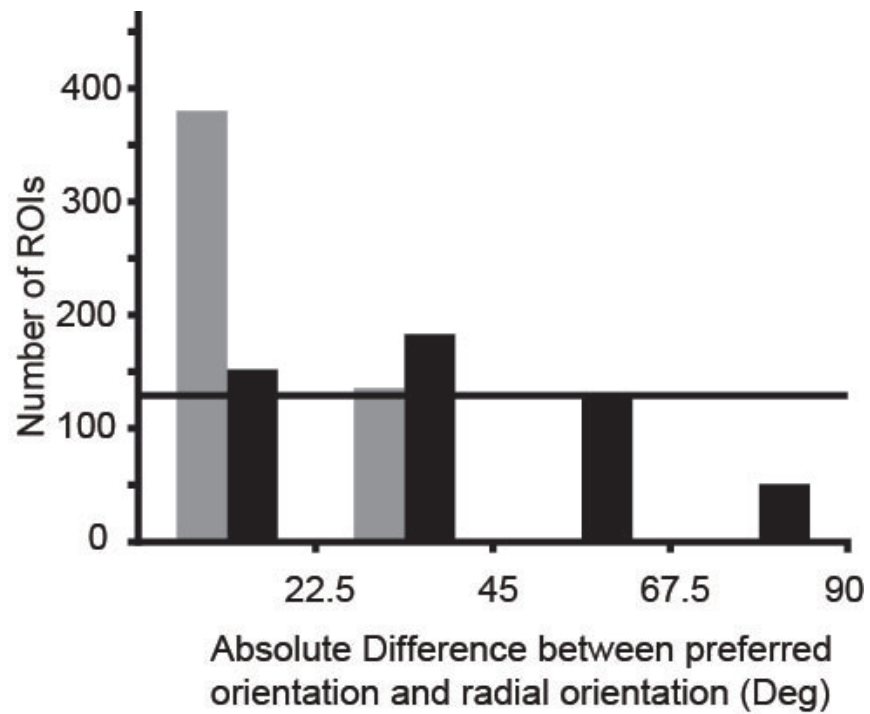


Figure 5.6: The distribution of absolute differences between the optimum orientation of the ROIs and their corresponding radial orientations. The horizontal line indicates the number of ROIs that would be present in each bin if the distribution were uniform.

Comparing the radial orientation and optimum orientation of single pixels

The difference between the optimum orientation of individual pixels and the mean radial orientation of the imaged area also showed that most pixels in the veridical condition were tuned to the radial orientation. Figure 7 shows the distribution of differences between the individual pixels and the mean radial orientation for the veridical and the filtered conditions. Once again, there was a strong peak between 0 and 22.5 degrees in the veridical condition. There was also a strong response between 22.5 and 45 degrees away from the radial angle. When compared with a uniform distribution (indicated by the horizontal line); the distribution of the differences for the veridical condition was significantly different (χ^2 -square=; df=; p).

The difference between the optimum orientation of individual pixels and the mean radial orientation of the imaged area in the filtered condition interestingly showed two peaks; one at the radial orientation and one at the orientation orthogonal to the radial orientation (see figure 7). This distribution was significantly different from the uniform distribution and also the distribution of differences for the veridical condition. When the distributions from the individual animals were fit with a circular Gaussian distribution, we observe two broadly tuned peaks at 0 degrees and 90 degrees, further emphasising the effect observed in the histograms.

We did not find any significant biases for horizontal and vertical orientations in either the ROI or the single pixel data.

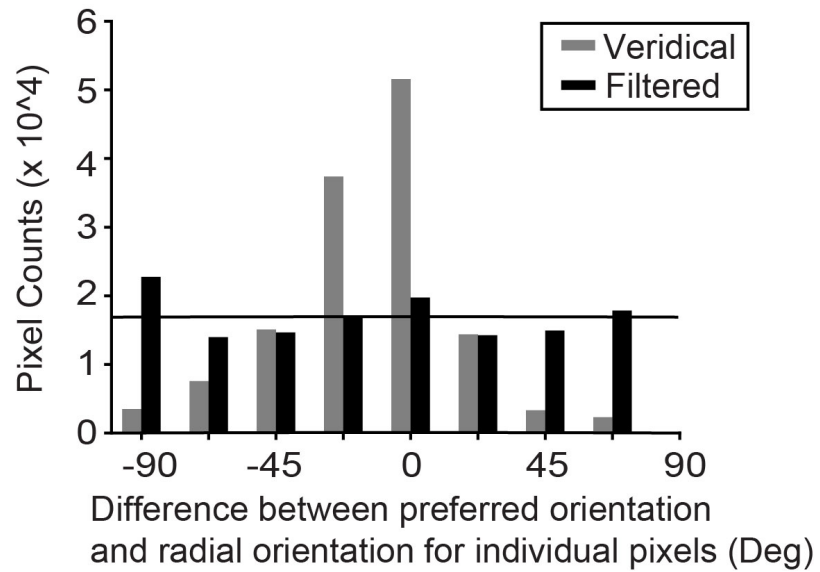


Figure 5.7: (a) The distribution of differences between the optimum orientation of single pixels and the mean radial orientation of the imaged area for the veridical and the filtered conditions. (b) The distribution of optimum orientation of the individual pixels grouped according to their preferred orientation. While there is a radial bias in the distribution of the pixels, there is no horizontal or vertical orientation biases.

One important issue that needs to be addressed is the sample size. Figure 7a shows that when looking at single pixels, the sample size is large (on the order of 10^5 pixels). The chi-square test, when performed on such a large sample will always give a significant result (REFERENCE). Therefore, to make sure that our single pixel results were not an artefact of sample size, we used random, repeated sampling with replacement methods. We used two sample sizes (either 40 or 1000) and sampled 1000 times (1000 trials). The results indicate that the radial bias observed in the veridical maps were strong and were observed even in the condition with sample size=40 (mean chi-square=; p=). There was also significant bias observed with sample size=1000. For the filtered condition, the biases for the radial and the orthogonal orientation were only visible when sample size was set at 1000. These results indicate that the radial bias in the veridical orientation maps was stronger than the biases observed in the filtered condition.

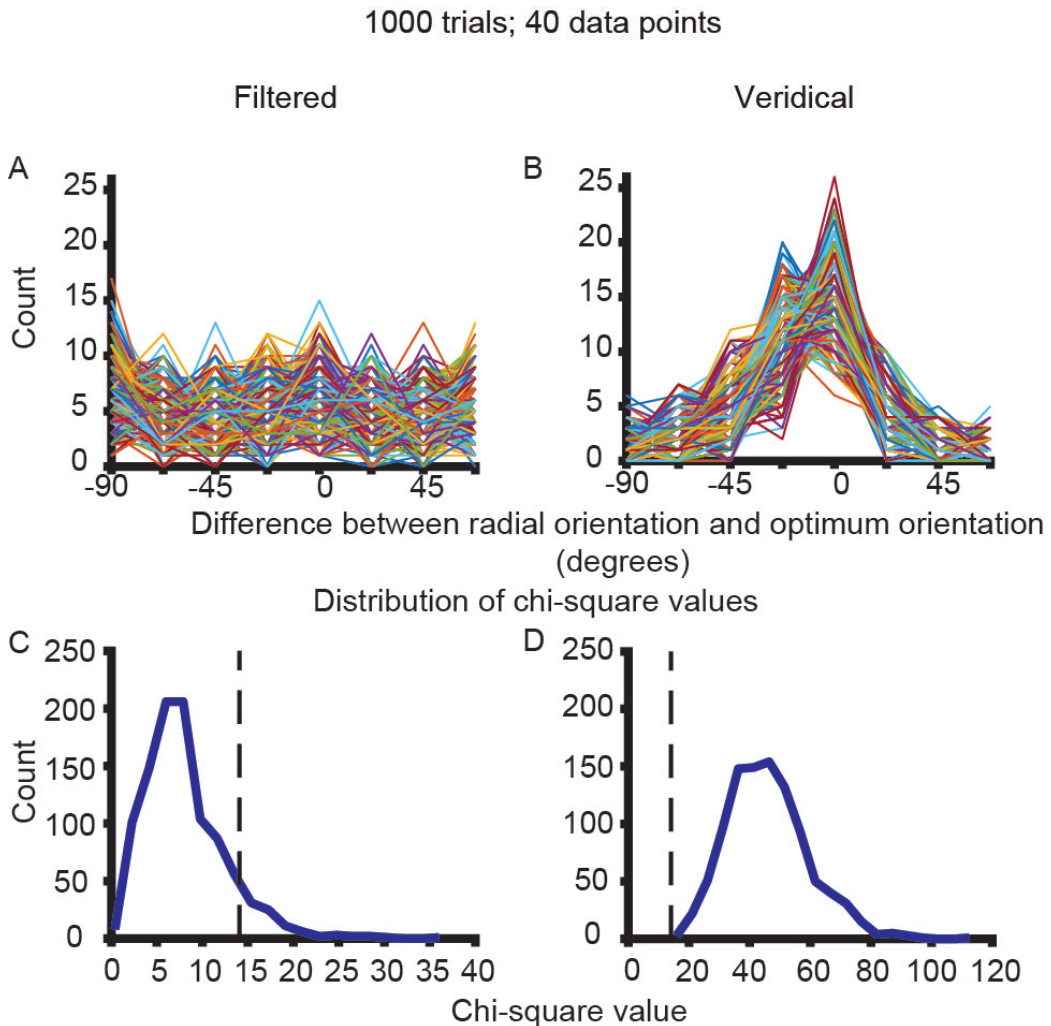


Figure 5.8: Repeated sampling with replacement. Sample size= 40. Number of trials= 1000. (a) and (b) are the distribution of single pixels randomly sampled from the distribution in figure 7a for the filtered and the veridical maps. Each line is the response of the pixel to a particular orientation. Parts (c) and (d) show the distribution of chi-square values for the individual neurons. The vertical line is the chi-square critical value for the given sample size and the degrees of freedom. For the filtered condition, most pixels were uniformly distributed. For the veridical condition, most pixels were significantly different from a uniform distribution.

1000 trials; 1000 data points

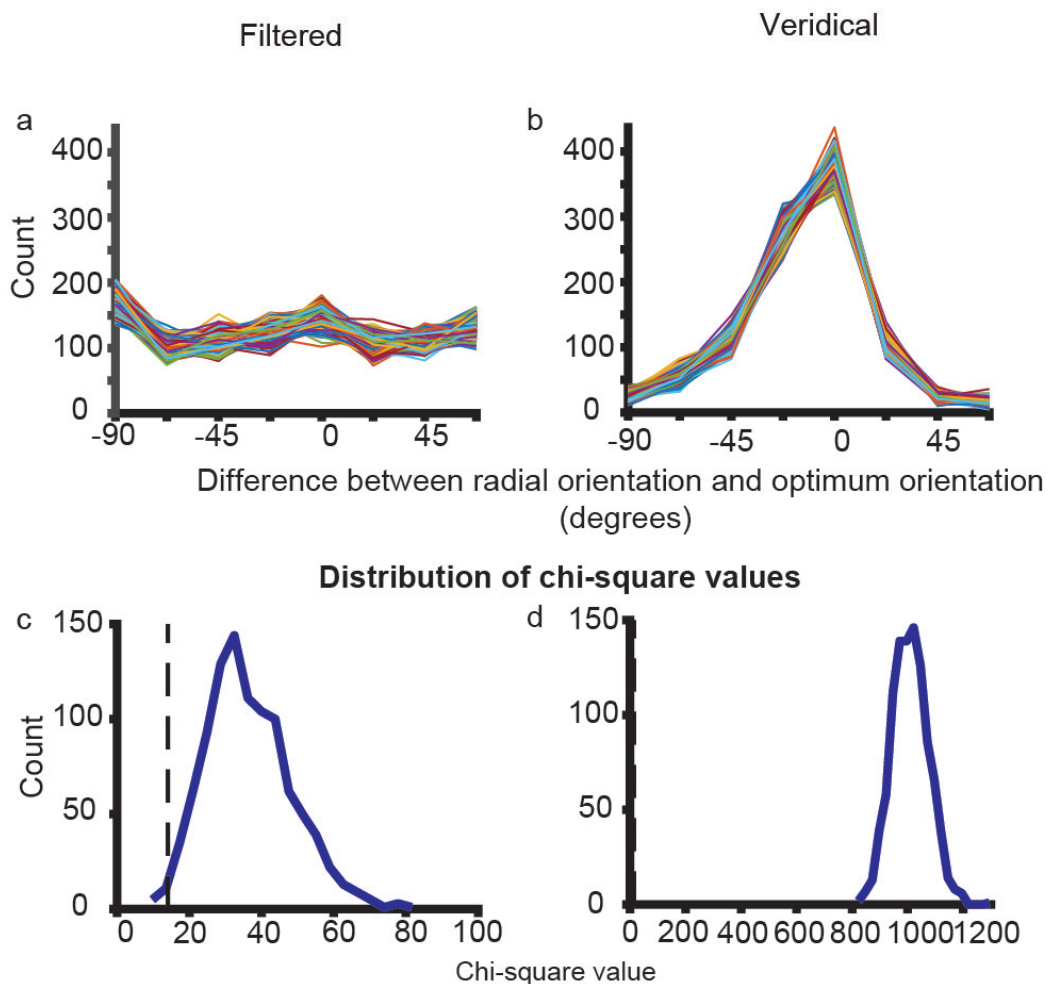


Figure 5.9: Repeated sampling with replacement. Sample size=1000. Number of trials= 1000. (a), (b), (c) and (d) are the same as in Figure 8. When the sample size is increased to a 1000 samples, both the filtered and veridical distributions were significantly different from a uniform distribution.

5.5 Discussion

Using optical imaging of intrinsic signals, we examined the inputs to the primary visual cortex and found that inputs to the primary visual cortex were strongly biased for the radial orientation. This fits in with the hypothesis that the orientation bias observed in the inputs were derived from biases observed in the retina rather than being generated by excitatory convergence of unoriented LGN inputs arranged in a row. However, we predicted that we would observe a bias for more than one of the cardinal orientations. This was not evident in the veridical signal. The filtered signal however, showed a bias to the radial orientation and the orientation orthogonal to the radial orientation. Not sure what this is about.

The mean difference between the radial angle and the optimum orientations in both the single pixel and ROI data is significantly different to 0. This indicates that the bias may not be entirely radial. However, this may not necessarily be the case. The experiment could have introduced systematic errors in various stages of data collection and analysis. The plotting of the foveal location is dependent on the visibility of the fovea when observed through the fundus camera. The visibility of the fovea itself is dependent on the optics which tends to deteriorate as the experiment progresses. The determination of the optic nerve head location is more robust. So, as long as an initial estimation of the optic nerve and the fovea are accurate, the subsequent positions of the fovea may be fairly accurately determined by plotting

the ON.

Receptive field estimation is also subject to error. Dow et al., allow for a half a degree jitter in both receptive field position and size of the receptive field. This compared with the fact that the ROI centres are extrapolated from the RF measurements could introduce another element of error. The formula used for extrapolation itself may not be exactly accurate in every animal and only allow for a crude extrapolation of receptive field position. This is because there are large variances in the organisation of the cortex between macaques and the estimates of RF location are based on standardised values. These differences may also introduce a systematic error in individual animals which could also add up.

Further, the single pixel optimum orientations were all compared to the mean radial angle of the imaged area. The radial angles of the receptive fields in the imaged area on area vary up to 30 degrees depending on the eccentricity of imaging. This introduces a further element of error in the measurements which contribute to a larger spread of differences in the single pixel data. Taking into account all these sources of error in determining the difference between the radial angle and optimum orientation, the actual radial bias in the data may be stronger than what has been reported.

During imaging, the tandem lens arrangement allows us to focus on a very narrow plane under the surface of the cortex while imaging. This depth is usually chosen on the basis of a few different factors. First, we need to see at what depth the signal we are looking for is strongest. The inputs to the

macaque cortex arrive in layer 4. Layer 4 is approximately 900 microns below the surface of the cortex. Imaging at these depths requires long wavelength filters. However, at these longer wavelengths, there is an increase in noise due to light scattering. The longest wavelengths that have been used for optical imaging are in the infrared range (710 nm) and at these wavelengths, the largest component of the signal is the noise caused by light scatter. Therefore, a trade-off needs to be made between depth and wavelength of the filter. In this study, we used a 630 nm filter and focussed our camera at a depth of 550-700 microns. This lets us image the bottom of layer 2/3. Layer 2/3 receives inputs from layer 4 but studies have shown that no further sharpening of orientation occurs in the parvocellular layer of layer 4 and there are also direct, koniocellular inputs to layer 2/3 in the macaque V1. Therefore, we can measure the pre-synaptic and synaptic inputs to layer 2/3 and still reliably make inferences on the nature of the inputs to the visual cortex itself.

Other optical imaging studies that have examined orientation biases have demonstrated the oblique effect; that is an underrepresentation of the oblique orientations in the primary visual cortex. These studies examined biases by grouping pixels based on their responses to different orientation but did not examine their relationship with their receptive field locations. Where the relationship between the receptive field location and the orientation of the neurons was, a radial bias was reported every time and at every stage of the visual system. In some cases, a horizontal bias has been reported due to the presence of the horizontal streak in the retina but even in these animals,

as one goes further away from the horizontal streak and the fovea, a strong radial bias is observed.

The radial bias might be an inevitable effect in the visual system. The prevalence of the radial bias has been higher in the peripheral visual system. Psychophysical studies have shown that the oblique effect is a very strong effect. The neurophysiological correlates of these oblique effects have been unclear but the radial bias in the periphery seems to be a result of the way in which the eye grows, automatically elongating the ganglion cell dendritic fields which influence their responses to oriented stimuli. The oblique effect in perception and the radial bias on the neural level may be unrelated phenomena.

Recent fMRI studies have demonstrated the radial bias in the visual cortex. Studies by Sasaki et al, etc have shown that when shown obliquely oriented stimulus, the activity in the BOLD response is higher than that observed for the horizontal and vertical stimuli. These studies show the radial bias on a larger and cruder spatial scale. Here, the radial bias in the cortex has been demonstrated at a smaller scale and a higher resolution, relating optimum orientations to receptive field locations rather than whole hemispheres. Sasaki et al. (2006) also demonstrate that the radial bias exists at higher visual areas. Our own results suggest that the inputs to the extrastriate areas from V1 will be tuned to the radial and the orthogonal orientations. These results along with our results indicate that the radial bias plays an important role in establishing cortical architecture.

If the range of orientation selectivity seen in the primary visual cortex originates from biases observed in the subcortical areas, we predicted that the inputs to the cortex may be broadly tuned to a small number of orientations. According to our results, one orientation dominated the inputs to the cortex. This does not necessarily mean that only one orientation is present in the inputs. The magnitude of the radial orientation signal is large and might overwhelm any smaller biases that may be observed. There would be no way to separate these signals on a spatial scale (as we usually do with the extracellular signal) without losing the information. A temporal means of segregating these signals may exist but again, our temporal resolution is not high enough to observe these changes. Our results only show that the inputs to the V1 are dominated by the radial orientation.

5.6 Conclusions

In this chapter, we aimed to examine if the inputs to the macaque primary visual cortex were predominantly tuned to a cardinal orientation. We used the unfiltered signal obtained from optical imaging of intrinsic signals in order to examine the larger scale organisation of the inputs. We imaged lower layer 2/3 and found that the presynaptic and synaptic activity were predominantly tuned to the radial orientation. The filtered signal was tuned to the radial and the orientation orthogonal to the radial orientation. Our results indicate that the columnar organisation observed in the primary visual cortex can be derived from biases observed in the subcortical areas and that excitatory convergence is not the source of orientation biases observed in the cortex.

Chapter 6

Orientation tuning in the Tree

Shrew superior colliculus

6.1 Abstract

Though theories of orientation selectivity suggest that orientation biases observed in V1 inputs are the result of excitatory convergence, studies have shown that bias in the inputs may be inherited from neurons in sub-cortical structures, especially the retina and the lateral geniculate nucleus (LGN). Congruent with this theory, retinal and LGN neurons have been shown to be tuned to orientation at higher spatial frequencies. If orientation selectivity arises from the retina, it should be evident in other targets of retinal projections. The superior colliculus (SC) is one such area. Here, I examined the orientation selectivity of SC neurons in tree shrews using thin bars and gratings of various spatial frequencies. I found that SC neurons show orientation tuning comparable to that observed in layer 4 of V1 in the tree shrews and orientation biases reported in the retina and the LGN of cats and macaques. This orientation selectivity was more evident at higher spatial frequencies. These results indicate that orientation tuning observed in the inputs to the cortex maybe generated from the orientation biases present in earlier visual areas.(Swisher et al., 2010)

6.2 Introduction

The theory of excitatory convergence (Hubel & Wiesel, 1962) suggests that orientation tuning in the primary visual cortex (V1) is derived from inputs from circular lateral geniculate nucleus (LGN) neurons that are arranged in a row converging on the V1 neuron. While this theory has garnered a lot of support, it has also been widely contested. In this chapter, I aim to examine one of the main assumptions of this theory: that subcortical neurons are unoriented.

A long list of studies have shown that orientation biases are present in subcortical structures. Levick and Thibos (1980) initially showed that retinal ganglion cells were tuned to orientation at higher spatial frequencies. These results have since been replicated in both cats and macaques at the level of the retina and the LGN. The retinal orientation biases are set to be derived from the natural growth pattern of the retina which elongates the dendritic fields. Given that orientation tuning is only observed at higher spatial frequencies and the fact that V1 neurons only respond at higher spatial frequencies, the degree of orientation tuning observed in the inputs to V1 can be generated by a mere sharpening of biased inputs.

Intracortical recordings in cat V1 have shown that the EPSPs observed in cortical neurons are tuned to orientation. Ferster (1986) argued that this orientation tuning may be explained by excitatory convergence. However, Pei et al (1994) showed that when the dynamics of orientation selectivity were

examined, the earlier EPSPs showed broader orientation tuning, similar to that reported in the LGN and retina. These broader signals were further tuned by inhibition observed as IPSPs (Pei et al., 1994). Both excitatory convergence and retinal orientation biases can explain orientation tuning of cortical inputs. However, only retinal bias model is consistent with the degree of orientation tuning of the inputs and the dynamics of the PSPs.

If the retina were the seed of orientation selectivity in the visual system, we should be able to detect orientation bias in parts of the brain that also receive inputs from the retina. The superior colliculus, which forms an alternate pathway to the visual cortex receives direct inputs from the retina. The superior colliculus neurons in cats and macaques however, prominently show no orientation biases. Recent studies have somewhat redeemed the SC, with rodent SC neurons showing sharp orientation tuning (eg: Ahmadlou et al., 2015). While there seems to be a different model of orientation selectivity and cortical organisation in the rodent, I believe that SC neurons that receive direct retinal inputs will also be tuned to orientation. This is because orientation tuning in subcortical areas are only present at higher spatial frequencies and studies that looked for orientation tuning in the SC did not take this into account. Here I looked at orientation biases in the tree shrew superior colliculus.

The tree shrew was chosen for a few important reasons, foremost of which is that it has a large, distinctly laminated superior colliculus that has been well characterised. Studies showed that as in macaques and cats, the su-

peripheral layers of the shrew SC receives direct input from the retina and has been implicated in form discrimination. These layers are also part of an independent pathway to the extrastriate cortex which is essential in form perception. However, unlike cats and macaques, in the tree shrew superior colliculus, a previous study showed that a small proportion of neurons in the superficial layers of the shrew SC had distinctly elongated fields (Albano et al., 1978). This study might have missed any small orientation biases as only fields that were 3 or more times longer than they were wide were classified as orientation selective.

Here I examined orientation biases in the SC neurons in attempt to show that orientation tuning in the inputs to the cortex was a reflection of the bias observed in the retina. We hypothesised that orientation tuning will be revealed in the superior colliculus at higher spatial frequencies. In particular:

- a) When using thin, moving bars, the neurons will be tuned to orientation and;
- b) When tested using gratings of different spatial frequencies and orientation, orientation tuning will be evident at higher spatial frequencies.

6.3 Methods

6.3.1 Electrophysiology

The superior colliculus in the tree shrew is large and well laminated structure and runs from the posterior edge of the brain to AP 2 (Horsley & Clarke coordinates, Tigges & Shanta, 1930). Following surgery, a craniotomy was per-

formed over the location of the superior colliculus. High impedance, lacquer coated tungsten microelectrodes (FHC Metal Microelectrodes Inc., Bowdoinham, ME, USA; impedance= 12-18 M Ω) were lowered into the brain and the signal was amplified and filtered (x 10,000 gain, bandpass filtered between 300-3000 Hz, AM systems amplifier) and fed into an audio speaker as well as an analog to digital converter (CED, Cambridge Systems, digitised at 22.5 kHz). The SC was identified by listening to the neuronal activity in the speaker. The data was recorded as a spike trace using the Spike 2 software. The spikes were templated and the spike timing exported as a text file. Further analysis was performed using custom MATLAB code.

6.3.2 Stimuli

A hand held projectoscope was initially used to demarcate the receptive field boundaries. Using this, the centre of the monitor was aligned with centre of the receptive field prior to stimulus presentation. Stimuli was presented using a Barco Reference Calibrator Plus monitor (Barco monitor; Barco Industries, Belgium, Frame Refresh Rate= 100 Hz) and the stimuli were generated using Visage (VSG, Cambridge Research Systems, Cambridge, UK) and custom Stimulus Description Language (SDL) scripts. The monitor had a mean luminance of 32.6 cdm $^{-2}$. In some experiments, an antiglare, anti static screen was used. The luminance when this screen was used was 17.4 cdm $^{-2}$. The monitor calibration was regularly checked using the PR-650 spectrophotometer (Photo Research, Palo Alto, CA, USA). While recording,

the monitor was placed at a distance of 114 cm from the eye.

For each SC neuron, the preferred stimulus orientation was initially measured using a thin moving bar. The bar was presented in 9 different orientations sweeping bi-directionally (a total of 18 orientations.). The background was a uniform gray screen. Depending on the polarity of the neurons, either a bright bar or a dark bar was used (contrast= 100 %). The bar was on average 8° long (ranging between 4 and 8 degrees) and 0.5° wide (ranging between 0.1 and 1 degree). The velocity of the bar was between 5 and 20 $^{\circ}$ /second.

Peri-stimulus-time-histograms (PSTHs) were generated online using the spike 2 () software. Based on the PSTHs generated following the presentation of the bar, the optimum orientation of the bar was determined as the orientation that gave the maximum response. This orientation was used for further testing.

The spatial frequency response to gratings were then measured. The animals were presented with drifting sine-wave gratings of varying spatial frequencies (TF= 4Hz, SF= 0 cpd to 2 cpd) at 4 different orientations (optimum, optimum + 90° , optimum+ 45° , optimum- 45°). In some cases, responses to a complete orientation tuning stimulus (16 directions/ 8 orientations) were recorded in order to further quantify the orientation response at a certain spatial frequency.

6.3.3 Data Analysis

Regardless of the stimulus presented, the following analysis was performed on the extracellular trace before any specific analysis. Spikes were templated based on their polarity, size and timing and the spike time and stimulus marker exported into text files. Using custom scripts in MATLAB (see Appendix), peri-stimulus-time-histograms (PSTHs) were constructed for each of the stimulus conditions. Spike density functions were created using a 3 bin moving average function. This SDF was used for further analysis.

For orientation tuning recorded using a bar, the peak response in the SDF for each direction was plotted on a polar diagram. The circular mean of this maximum response and the corresponding direction was calculated using the following formula:

The circular variance (CV) and the orientation selectivity index(OSI) were also calculated as follows:

$$CV =$$

$$OSI =$$

For the gratings, the Discrete Fourier Transform (DFT) of the spike density function was calculated using the MATLAB fast fourier transform algorithm. The F1 and the F0 component were calculated as mentioned in the general methods. The F0:F1 ratio was calculated at the peak spatial frequency. The peak spatial frequency is the maximum spatial frequency after which both the F0 and the F1 decrease. If the F0 response was smaller than the F1 response (ie. the ratio was less than 1), the cell was deemed to be

X-like and the magnitude of the first harmonic component of the response was used for further analysis. If the ratio was greater than 1, the cell was considered non-linear and the F0 component was used.

The spatial frequency tuning at the optimum and orthogonal orientations were calculated by linearly interpolating between the data points. The bandwidth during which the superior colliculus neurons responded for the optimum orientation but not for the orthogonal orientation was calculated. In order to do this, a minimum response was first defined as the response rate at the spatial frequency where the response between the optimum and orthogonal orientations were no longer significantly different. The spatial frequency where the response rate for the optimum and orthogonal orientations first reach the minimum response was termed the optimum SF cutoff and orthogonal SF cutoff. The difference between SF cutoff for the optimum and orthogonal spatial frequencies were calculated.

6.4 Results

Anatomical location of units

A total of 22 units (5 tracks in 3 Tree Shrews) were recorded from. The laminar position of all the units were determined by reconstructing the electrode tracks using electrolytic lesions. The photomicrograph from one of the Nissl stained sections in one of the tree shrews is presented in figure 6.1a. In this section, lesions made in 2 separate tracks are visible (red arrow points to one

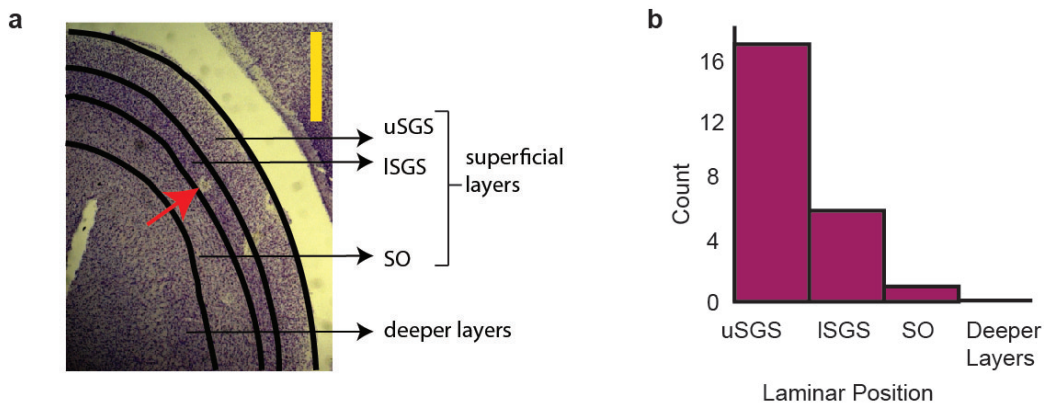


Figure 6.1: Histology. a) A section of tree shrew superior colliculus showing electrolytic lesions. Red arrow points to an electrolytic lesion. Scale bar (yellow vertical line) denotes 1000 m. b) A summary of laminar position of recorded units in the superior colliculus. Abbreviations: uSGS- upper Stratum Griseum Superficiale; ISGS- lower Stratum Griseum Superficiale; SO- Stratum Opticum.

of them). The different layers of the tree shrew SC are marked. The superficial layers are further distinguished. Electrode reconstruction was completed in all animals and the laminar position of each of the neurons is shown in Figure 6.1b. All the neurons we recorded from were located in the superficial layers with the majority being in the Stratum Griseum Superficiale (SGS) where the retinal inputs terminate.

Orientation Selectivity

The response of a representative neuron to moving bars of different orientations and the corresponding orientation tuning curves are presented in figure showed in figure 6.2. The response was the average of 10 trials and the small error bars suggest that the response was highly consistent (Error bars = \pm sem). The CV of this neurons was 0.82. The median CV of all the neurons in our sample was 0.82 with a range of [0.29, 0.94]. Any neuron with CV greater than 0.9 was considered not selective to orientation. Two neurons had a CV greater than 0.9 and were excluded from further analysis. The orientation tuning curves of the most selective, least selective neuron with Cv less than 0.9 and the least selective neuron in the entire sample are presented in figure 6.3. The histogram of all the circular variances are presented in figure 6.4.

Spatial Frequency Tuning

When the spatial frequency tuning response of the neuron at different orientations was observed, 13 of 16 neurons were orientation tuned at higher spatial frequencies. The spatial frequency response of an example neuron at the optimum and the orthogonal orientations is presented in figure 6.5a. The response is the F0 component of the FFT. The gray shaded area represents the spatial frequnecies where the neuron still responds to the optimum orientation but no longer responds to the orthogonal orientation (ie. the neuron is orientation tuned). The upper limit of the gray shaded area (the dotted line to the right) is the cut off spatial frequency at the optimum orientation.

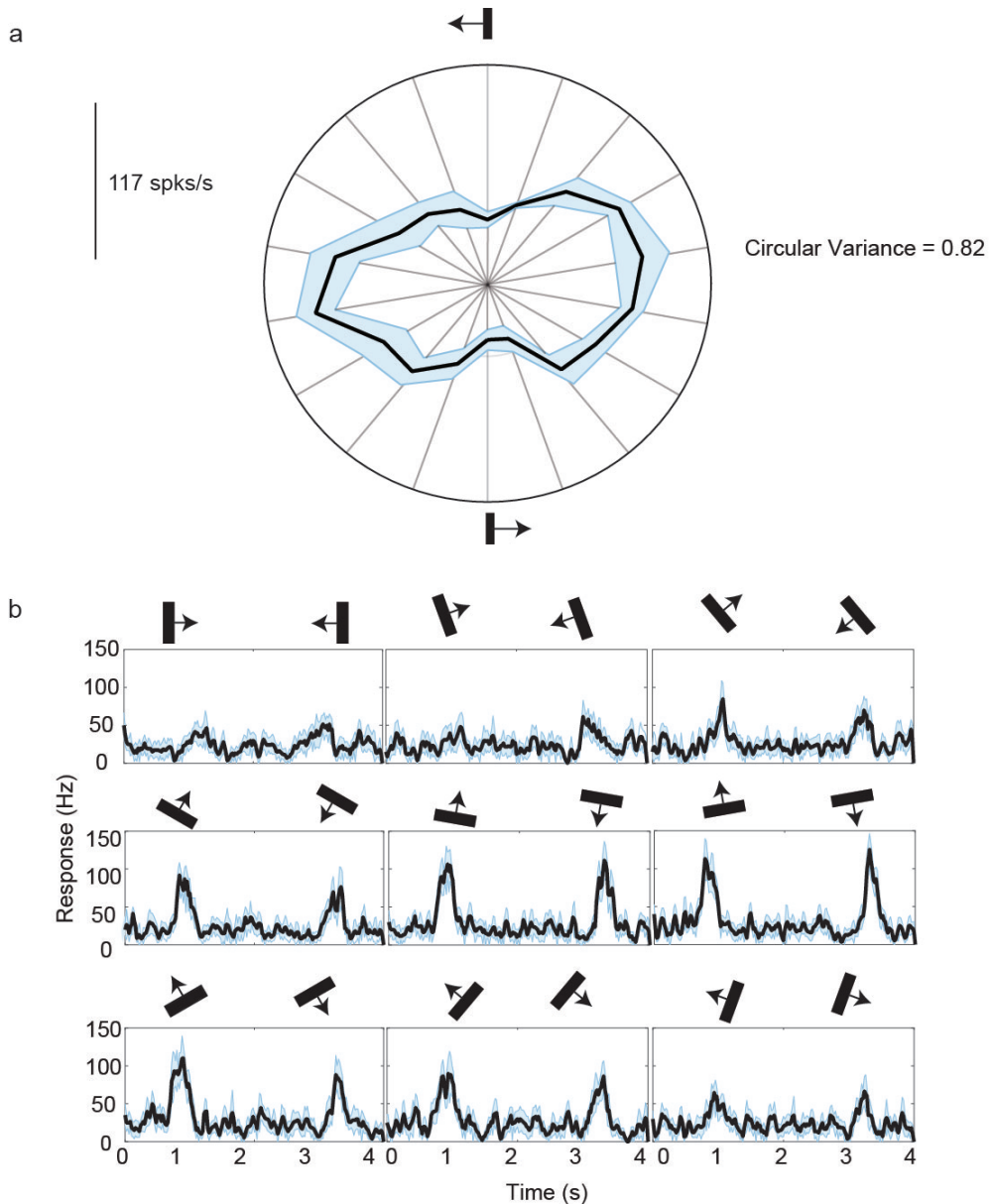


Figure 6.2: Orientation response of an example cell. a) The polar plot of the orientation responses of a neuron in the tree shrew superior colliculus. Each spoke represents an orientation presented. The circular variance of this neuron is 0.82. This was also our median circular variance. b) The spike density functions for different orientations for the neuron whose polar plot is shown in a. The orientation and direction of movement of the bar is shown above the trace.

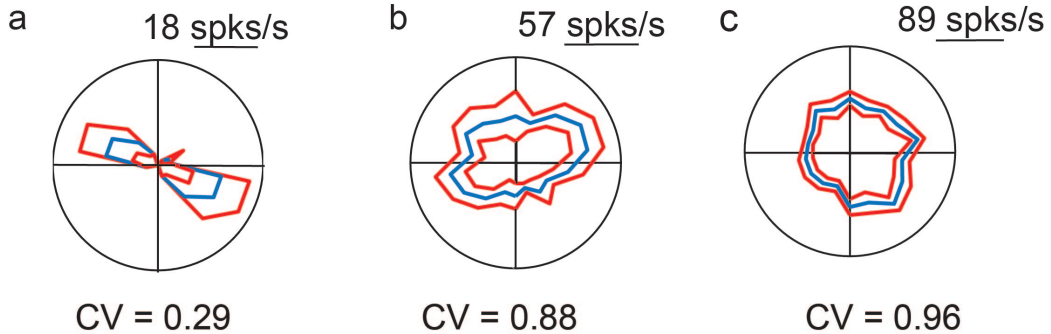


Figure 6.3: Polar plot showing the orientation tuning of the bar. Error bars denote Standard error. Orientation tuning curves of the sharpest (a) and the least tuned (b) neurons included in our analysis. (c) was the least tuned neuron in our sample

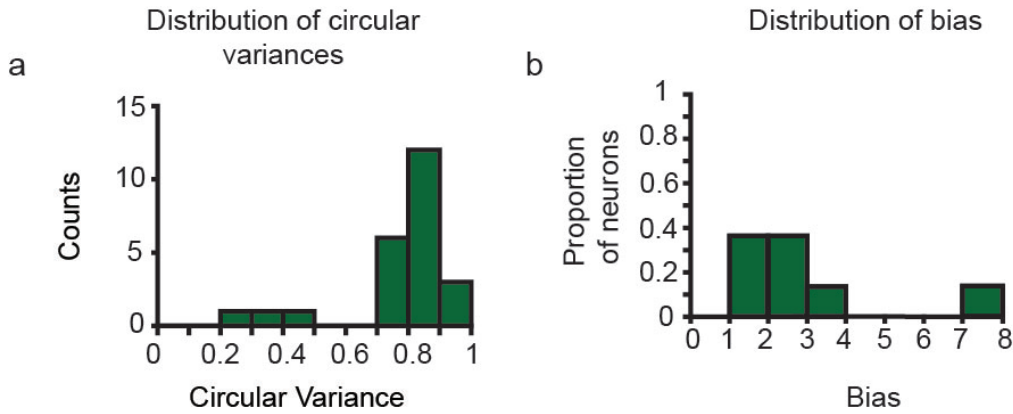


Figure 6.4: Circular variances: (a) This figure shows the distribution of circular variances of all neurons. Most of the tuned neurons have a CV between 0.7 and 0.9. The apparent second peak is discussed further in the discussion (b) This figure shows the laminar position of the individual neurons plotted against the circular variances. Apart from the three neurons in the upper SGS that are sharply tuned to orientation, there doesn't seem to be any differences in the orientation selectivity between the upper and lower SGS. There was an inadequate sample from the SO for comparison.

The sf corresponding to the lower limit of the shaded gray area is the cut off spatial frequency. The difference in response between the optimum and non-optimum orientation cut off frequencies was calculated. These results for the group are presented in figure 6.6 a. On average, the response to the orthogonal orientation reached the minimum 0.5 cpd before the response to the optimum orientation; with the 95 percent CI= [0.4, 0.6].

The OSI at each of the spatial frequencies for the example neuron is plotted in figure 6.5 b and the group results are presented in figure 6.6 b. The neuron exhibited the highest bias close to the cut off frequency at the orthogonal orientation.

6.5 Discussion

The results of this study demonstrate that neurons in the superior layers of the superior colliculus are tuned to orientation at higher spatial frequencies. This finding in combination with other reports of orientation biases in sub-cortical areas renders one of the key assumption of the excitatory convergence model that subcortical neurons have circular, unoriented receptive fields which then requires the arrangement of their receptive fields in a row to give rise to orientation tuning incorrect. Not only do tuned cortical inputs then pave the way for intracortical inhibition to sharpen orientation selectivity, they also abet the development of cortical architecture.

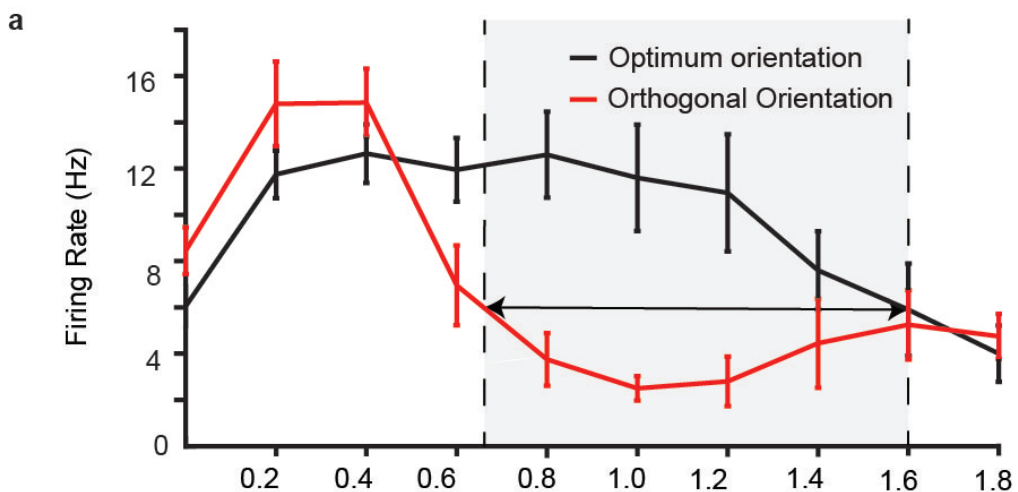


Figure 6.5: Example SF tuning curves for optimal and orthogonal orientations. The cut-off frequency at the optimal orientation is the SF at which the response at optimal orientation is no longer significantly different from the response at orthogonal orientation. The response at the cut-off frequency for optimum orientation is called the minimum response. For the orthogonal orientation, the cut-off frequency was the SF at which minimum response was first reached.

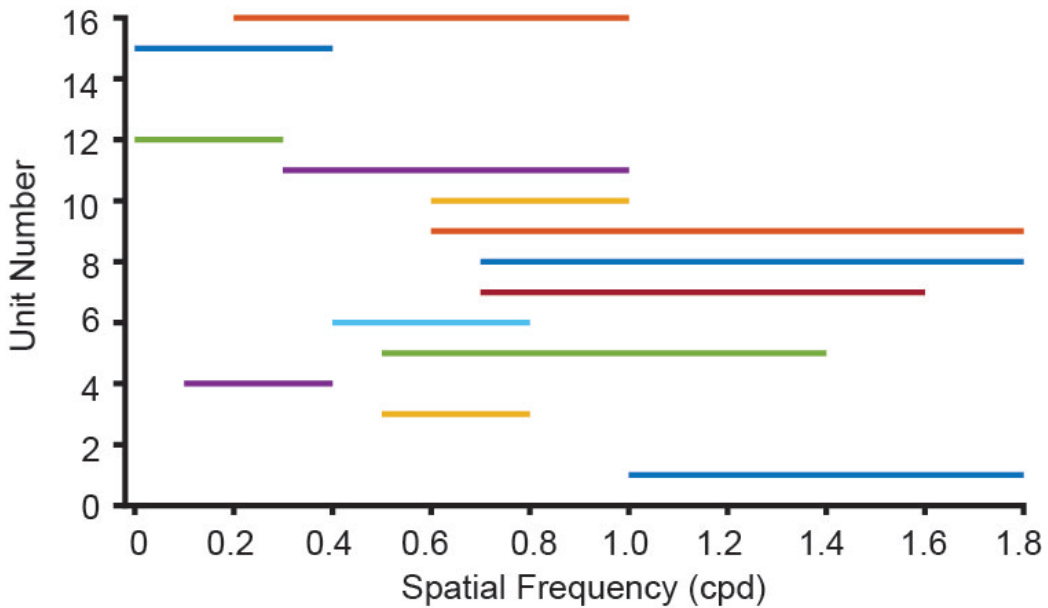


Figure 6.6: The difference between the cut-off frequencies for the optimum and orthogonal orientations for 16 units is shown in Figure 3b.

6.5.1 Anatomical Relevance

The histology confirmed that all the units that were recorded from the superficial layers of the superior colliculus. While the superior colliculus receives information from all the sensory modalities, the superficial layers receive direct input from the retina and feedback projections from the primary visual cortex. They also project to extrastriate visual areas. Lesion studies have shown that when the shrew SC is lesioned, form perception is affected. In Studies where the primary visual cortex of the tree shrew was ablated while keeping the SC and extra-striate visual areas intact showed that tree shrews could still consciously perceive form information further implicating the superficial layers of the shrew SC in playing an important role in perception.

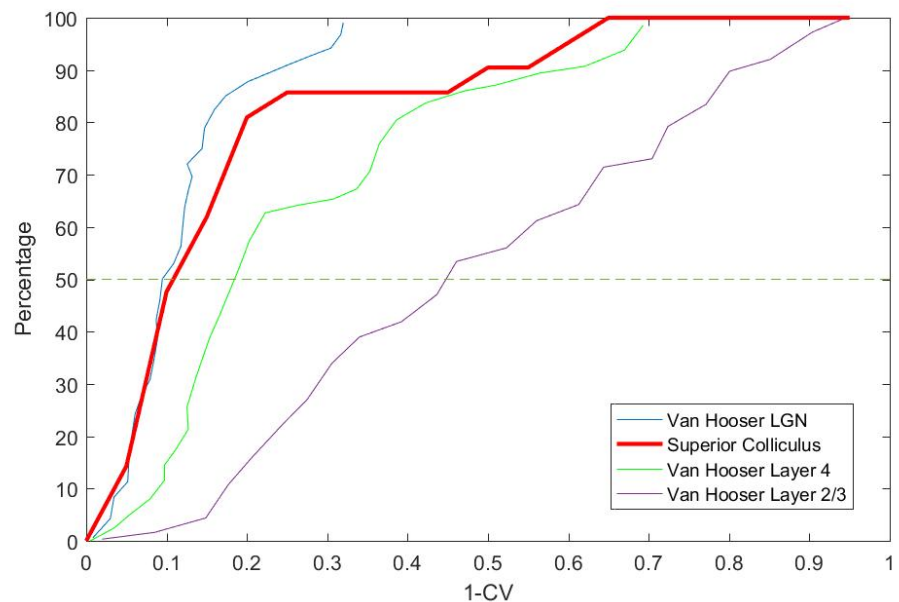


Figure 6.7: Comparison of the Superior Colliculus vs neurons in the geniculostriate system (data collected by Van Hooser et al., 2013)

Given its position in this alternate visual pathway and its role in form perception, it is surprising that orientation tuning has not been reported in the Superior Colliculus. Where it has been reported, like in the case of the tree shrews, a very small proportion of neurons have said to be tuned to orientation. These neurons have also been reported in the superficial areas of the superior colliculus.

6.5.2 Comparison with previous tree shrew studies

In their earlier paper, Albano et al., 1978 suggested that less than 10% of the neurons had elongated receptive fields. However, in our study, 90% of our neurons were orientation selective. It is important to make a distinction in these two results. While they may sound like it, these results are not entirely contradictory. In their study, Albano et al tested the elongation of the receptive fields. That is, using the neuronal responses, they plotted the receptive field boundaries of neurons and concluded that any neuron that had an aspect ratio of 3:1 had elongated receptive field. In this study on the other hand, we used the response of the neurons to bars and gratings of different orientations. Studies have shown that only a slight receptive field elongation is required for a neuron to give orientation specific response. Albano et al may have simply not detected smaller effects which have been reported in the retina and LGN due to their conservative criterion for classifying a neuron as orientation selective.

Another reason Albano et al., 1978 may not have detected the extent of

orientation tuning in the shrew SC could be the stimulus used. As mentioned earlier, bars and gratings were used in this study. Albano et al also used these stimuli however, only one paper was published (1974) in the cat retina indicating that orientation tuning was detected at higher spatial frequencies (Hammond, 1974). However, in the eighties, a lot of papers were published revealing the spatial frequency dependence of orientation tuning. The lack of this knowledge may also be one of the reasons why the orientation selectivity in the superior colliculus was missed.

Van Hooser et al., 2013 published a comprehensive set of data on the transformation of the receptive fields from the lateral geniculate nucleus to the layer 4 (input layer) to layer 2/3 of the tree shrew visual system. The orientation tuning of the superior colliculus neurons are plotted in relation to the geniculate, layer 4 and layer 2/3 neurons in the tree shrew in figure 6.7. This comparison indicates that the orientation biases observed in the superior colliculus are similar to those observed in the LGN of the tree shrew, with approximately 85% of the SC neurons having similar orientation tuning to the LGN neurons in the Van Hooser study. There is a tendency in our data for around 15% of neurons to have sharper orientation tuning than those exhibited in the LGN, closer to those seen in the cortex. While the neurons in the upper and lower SGS receive predominantly retinal inputs, there are also neurons which receive feedback projections from the primary visual cortex. These neurons could be one of the few neurons that receive cortical feedback. This can also be seen in figure 6.4 where the distribution

of circular variance seems to be in two different groups. However, the sample size in this study is too small to comment on this segregation.

6.5.3 Comparison with previous superior colliculus studies

The superior colliculus being a large, well laminated organ in most species was intensely studied for a while. The studies conducted in the superficial layers of the cat and macaque superior colliculus showed that the superior colliculus neurons were direction selective whereas no orientation selectivity was observed. In this sense, the SC was previously compared to the LGN both sub-cortical areas receiving unoriented input and relaying unoriented inputs to different pathways. However, the realisation that superior colliculus neurons may not be tuned to orientation at higher spatial frequencies seems to have not occurred in people who have investigated it. Recent rodent studies have shown that the rodent superior colliculus shows sharp orientation selectivity. Previous studies have demonstrated that the tree shrew superior colliculus is similar to the macaque visual system and the SC makes similar connections to extrastriate cortical areas in the macaque and the shrews. So it is possible that orientation biases are present in these animals as well and will be revealed when tested with higher spatial frequency stimuli.

6.5.4 Comparison with the geniculostriate system of cats and macaques

One of the prominent paper published investigating the spatial frequency dependence of orientation tuning in the retinal ganglion cells of cats was Levick and Thibos (1982). They characterised the way orientation tuning varied with spatial frequency. In the following paragraph, I will evaluate our results in the context of the responses of retinal ganglion cells.

One of the two key findings of Levick and Thibos was that RGCs were tuned to orientation at higher spatial frequencies. They also found that in some cases, at lower spatial frequencies, the neuron responded better at the orthogonal orientation compared to optimal orientation. They also reported that the degree of orientation selectivity (reported as orientation bias) was the maximum close to the threshold. In the tree shrew SC, all these findings hold true. A close examination of Fig: 6.5 shows that orientation tuning is observed at higher spatial frequencies. Figure 6.5 b also shows that the orientation bias was the maximum close to the threshold. Figure 6.6b also demonstrates this. Figure 6.5 is also only one example of a case where the neuron was biased for the orthogonal orientation at lower spatial frequencies. Neuron being oriented to different orientations at lower spatial frequencies was also a common finding in the superior colliculus. But the optimum orientation of the neuron as measured using bars was the orientation for which the SF cut-off was the highest in all cases. These properties have also

been more universally demonstrated in the retina of macaques and also the LGN of cats and macaques, further indicating that the orientation biases have a common, retinal ancestry.

6.5.5 Conclusion

In this chapter, I set out to examine if one of the key assumptions of the excitatory convergence model that subcortical neurons had circular receptive fields was indeed true. Previous studies in the retina and the lateral geniculate nuclei of cats and macaques have shown that subcortical neurons were tuned to orientation at higher spatial frequencies. I hypothesised that the tree shrew SC neurons would also be tuned to orientation at higher spatial frequencies. When examined with thin bars and gratings of increasing spatial frequencies, SC neurons were indeed tuned to orientation. These orientation tuned inputs may then be sharpened by intracortical inhibition to generate the sharp orientation selectivity we see in the primary visual cortex. Inputs tuned broadly to a small number of orientations could also give rise to the organisation of cortical columns. Finally, establishing orientation biases in the retina also reduces the functional redundancy of establishing orientation tuning in the different parallel pathways.

Part II

Insights from the Tree Shrew Primary Visual Cortex

References

Swisher, J. D., Gatenby, J. C., Gore, J. C., Wolfe, B. a., Moon, C.-H., Kim, S.-G., & Tong, F. (2010, jan). Multiscale pattern analysis of orientation-selective activity in the primary visual cortex. *The Journal of neuroscience : the official journal of the Society for Neuroscience*, 30(1), 325–30. Retrieved from <http://www.ncbi.nlm.nih.gov/pmc/articles/PMC2823298/> doi: 10.1523/JNEUROSCI.4811-09.2010